2-Dimensional networks assembled using 4'-functionalized 4,2':6',4''-terpyridines and $Co(NCS)_2$ †

Y. Maximilian Klein, Alessandro Prescimone, Edwin C. Constable* and Catherine E. Housecroft*

Department of Chemistry, University of Basel, Spitalstrasse 51, 4056 Basel, Switzerland

E-mail: catherine.housecroft@unibas.ch

†This paper is dedicated to our longstanding friend and colleague Malcolm H. Chisholm on the occasion of his 70th birthday.

Abstract

A series of 2-dimensional (4,4) nets formed in reactions of $Co(NCS)_2$ with divergent 4'-functionalized-4,2':6',4''-terpyridine ligands is reported, and the effects of the 4'-substituent R (ligand **1**, R = ^{t}Bu; **5**, R = MeO; **6**, R = EtO; **7**, R = ^{n}PrO) on the packing of the nets are described. The 2D-coordination networks in $[\{Co(NCS)_2(\mathbf{6})_2\}\cdot 4CHCl_3]_n$ and $[\{Co(NCS)_2(\mathbf{7})_2\}\cdot 4CHCl_3]_n$ are essentially isostructural. On going to $[\{Co_2(NCS)_4(\mathbf{5})_4\}\cdot 2CHCl_3\cdot 1.5MeOH]_n$, modification of both the geometry of the rhombuses that comprise the network, and the packing occurs. All three structures feature head-to-tail π-stacking of 4'-(4-alkoxyphenyl) units, but with variation in their relative orientations. In contrast, $[\{Co(NCS)_2(\mathbf{1})_2\}\cdot 0.5H_2O]_n$ comprises double layers of (4,4) nets with hydrophobic coatings of *tert*-butyl groups, leading to alternating wide and close spacings between adjacent nets.

Keywords: cobalt; 4,2':6',4''-terpyridine; coordination polymer; coordination network; substituent effects

1. Introduction

The coordination chemistry of 4,2':6',4''-terpyridines has seen a significant growth since the first coordination polymer of 4,2':6',4''-terpyridine (4,2':6',4''-tpy) was reported [1]. A 4,2':6',4''-tpy binds metal ions through only the two outer nitrogen atoms and therefore possesses a divergent donor set (Scheme 1). 1-Dimensional chains tend to dominate the coordination polymers formed using 4,2':6',4''-tpy ligands as linkers [2] but, in part, this has been due to the popularity of zinc as the metal node, either in reactions with zinc(II) halides or zinc acetate; the latter typically results in linear $\{Zn_2(\mu\text{-}OAc)_4\}$ nodes. To encourage the formation of 2- or 3-dimensional architectures, the 4,2':6',4''-tpy ligand can be modified by introducing metal-binding domains in the 4'-position. This is readily done using Kröhnke [3] or Wang and Hanan [4] synthetic approaches. Examples of such 4'-donors are pyridinyl [5,6], carboxylato [7,8,9] or diphenylphosphino [10] groups. Other approaches are to choose metal ions with higher coordination numbers [11] or to design ligands with multiple 4,2':6',4''-tpy domains [12,13,14,15]. Recently, we extended this latter strategy to a linker bearing two 3,2':6',3''-tpy domains and showed that with $Co(NCS)_2$, a $\{4^2.8^4\}$ lvt net is produced [16]. The assembly of this 3-dimensional network was a consequence of using a ligand with two, divergent terpyridine domains (a 4-connecting node) and a metal ion that can also function as a 4-connecting node. Following this success and the results of previous studies in which 2-dimensional nets were obtained from reactions of $Co(NCS)_2$ with ligands **1–4** (Scheme 1) [17,18], we have extended our investigations of coordination networks assembled from $Co(NCS)_2$ and 4'-functionalized 4,2':6',4''-tpy ligands.

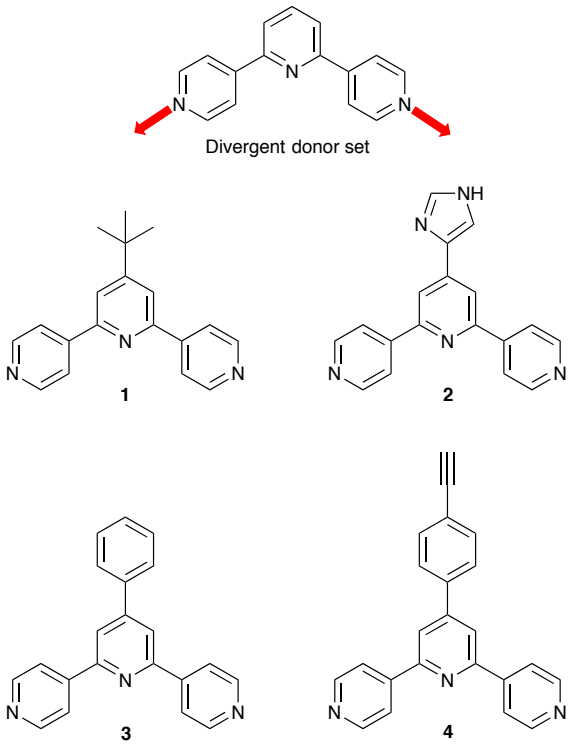

Scheme 1. Definition of 4,2':6',4"-tpy as a divergent ligand, and 4,2':6',4"-tpys previously shown to form 2-dimensional nets with $Co(NCS)_2$ [17,18].

Cobalt(II) thiocyanate combines with a wide range of ditopic ligands containing pyridine metal-binding units. Scheme 2 shows examples of pyridine-donor ligands which form 2- or 3-dimensional architectures with $Co(NCS)_2$. In most cases the cobalt centre acts as a 4-connecting node (octahedral with *trans*-$[NCS]^-$ ligands), although an interesting departure from this is found in $[Co_2(NCS)_4(bpa)_3]_n$ (bpa, Scheme 2) which contains cobalt as both 2- and 4-connecting nodes [19]. The ligands included in Scheme 2 possess rather rigid backbones and, in common with 4,2':6',4"-tpy, present divergent sets of *N*-donor atoms. The combination of a divergent *N,N'*-linker with a 4-connecting metal node should be preorganized for the formation of a 2-dimensional (4,4) net, and indeed, this is observed for the combinations of $Co(NCS)_2$ with the rod-like ligands 4,4'-bpy, 2,2'-bi(1,6-naphthyridine), bpet, bpo, bpt, bpe, mbpe, mppe and bpaz shown in Scheme 2 [20–29]; inclined interpenetration of (4,4) nets is observed in several cases [22,23,24]. However, while the reaction of $Co(NCS)_2$ with 4,4'-bpy gives a (4,4) net [30],

it has also been shown to give a 1-dimensional chain in $[\{Co(NCS)_2(\mu\text{-}4,4'\text{-bpy})_2(4,4'\text{-bpy})_2\}\cdot 2DMF]_n$ in which half of the 4,4'-bpy ligands are monodentate and the solvent is implicated in controlling the assembly [31]. An analogous linear chain is seen in $[\{Co(NCS)_2(\mu\text{-}4,4'\text{-bpy})_2(bpaz)_2\}\cdot H_2O]_n$ [32] (see Scheme 2 for bpaz). The advantages of the divergent mode of 4,2':6',4''-tpy over the convergent donor set in the more common isomer 2,2':6',2''-tpy is seen by comparing the assemblies formed between $Co(NCS)_2$ and either 4'-(4-py)-2,2':6',2''-tpy or tpt (Scheme 2); the chelating nature of the 2,2':6',2''-tpy domain is restrictive and $[Co(NCS)_2(4'\text{-}(4\text{-py})\text{-}2,2':6',2''\text{-tpy})]_n$ forms a linear chain [33] whereas reaction between tpt and $Co(NCS)_2$ gives 3-dimensional networks [34,35].

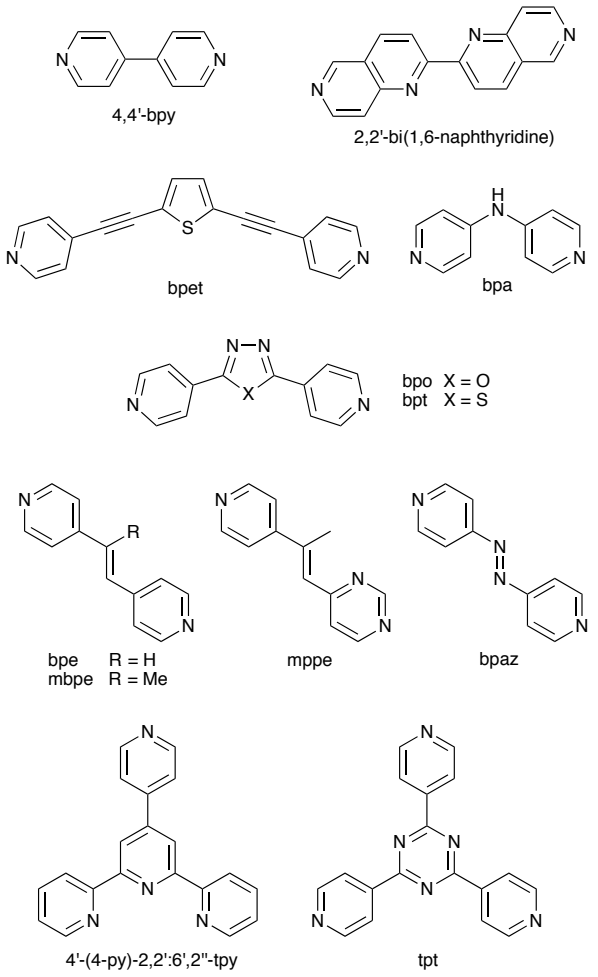

Scheme 2. Representative pyridine-containing ligands which form 2- or 3-dimensional architectures with $Co(NCS)_2$.

We now report a series of 2-dimensional nets formed when $Co(NCS)_2$ reacts with the four 4'-functionalized 4,2':6',4''-tpy ligands **1** (Scheme 1) and **5–7** (Scheme 3) and discuss variation in packing of the sheets as a function of the 4'-substituent.

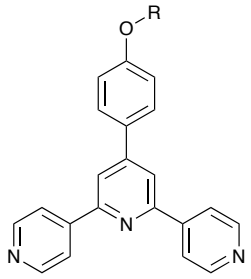

5 R = Me
6 R = Et
7 R = ^{n}Pr

Scheme 3. Structures of ligands **5**–**7**.

2. Experimental

2.1 Ligands

Ligands **1** and **5–7** were prepared as previously described [[17],36].

2.2 $[\{Co_2(NCS)_4(\mathbf{5})_4\}\cdot 2CHCl_3\cdot 1.5MeOH]_n$

A MeOH (8 mL) solution of $Co(NCS)_2$ (5.25 mg, 0.03 mmol) was layered over a $CHCl_3$ (5 mL) solution of **5** (30.5 mg, 0.09 mmol) and left to stand at room temperature. Pink crystals of $[\{Co_2(NCS)_4(\mathbf{5})_4\}\cdot 2CHCl_3\cdot 1.5MeOH]_n$ (14.8 mg, 0.007 mmol, 47% based on Co) were obtained after 1-2 weeks. Bulk sample analysis: see text.

2.3 $[\{Co(NCS)_2(\mathbf{6})_2\}\cdot 4CHCl_3]_n$

A MeOH (8 mL) solution of $Co(NCS)_2$ (5.25 mg, 0.03 mmol) was layered over a $CHCl_3$ (5 mL) solution of **6** (10.6 mg, 0.03 mmol) and left to stand at room temperature. Pink crystals of $[\{Co(NCS)(\mathbf{6})\}\cdot 2CHCl_3]_n$ (3.0 mg, 0.002 mmol, 7% based on Co) were obtained after 1-2 weeks. Bulk sample analysis: see text.

*2.4 [{Co(NCS)$_2$(**7**)$_2$}·4CHCl$_3$]$_n$*

A MeOH (8 mL) solution of $Co(NCS)_2$ (5.25 mg, 0.03 mmol) was layered over a $CHCl_3$ (5 mL) solution of **7** (22.0 mg, 0.06 mmol) and left to stand at room temperature. Pink crystals of [{$Co(NCS)_2$(**7**)$_2$}·4$CHCl_3$]$_n$ (12.0 mg, 0.009 mmol, 29% based on Co) were obtained after 1-2 weeks. Bulk sample analysis: see text.

*2.5 [{Co(NCS)$_2$(**1**)$_2$}·0.5H$_2$O]$_n$*

A MeOH (8 mL) solution of $Co(NCS)_2$ (3.50 mg, 0.02 mmol) was layered over a $CHCl_3$ (5 mL) solution of **1** (17.4 mmol, 0.06 mmol) and left to stand at room temperature. Pink crystals of [{$Co(NCS)_2$(**1**)$_2$}·0.5H_2O]$_n$ (5.1 mg, 0.007 mmol, 33% based on Co) were obtained after 1-2 weeks. See text for characterization of the bulk sample by powder X-ray diffraction.

2.6 Crystal structure determinations

Crystallographic data were collected on a Bruker-Nonius Kappa APEX diffractometer, and data reduction, solution and refinement used APEX2 [37] and CRYSTALS [38]. Powder diffraction data were collected on a Stoe Stadi P powder diffractometer. Structural diagrams and structural analysis were carried out using Mercury v. 3.5.1 [39,40] and TOPOS [41]. The solvent region in [{$Co(NCS)_2$(**7**)$_2$}·4$CHCl_3$]$_n$ was treated using the program SQUEEZE [42], and the electron density removed was equated to two extra molecules of $CHCl_3$ per Co atom which were added to the molecular formula.

*2.7 [{Co$_2$(NCS)$_4$(**5**)$_4$}·2CHCl$_3$·1.5MeOH]$_n$*

$C_{95.50}H_{76}Cl_6Co_2N_{16}O_{5.50}S_4$, M = 1994.60, pink block, triclinic, space group P–1, a = 13.7002(12), b = 18.0092(15), c = 20.4275(17) Å, α = 98.287(4), β = 99.998(3), γ =

110.322(3)°, U = 4539.1(4) Å^3, Z = 2, D_c = 1.459 Mg m^{-3}, μ(Cu-Kα) = 5.869 mm^{-1}, T = 123 K. Total 68836 reflections, 16258 unique, R_{int} = 0.036. Refinement of 15530 reflections (1196 parameters) with I >2σ (I) converged at final R1 = 0.1166 (R1 all data = 0.1191), wR2 = 0.2862 (wR2 all data = 0.2867), gof = 0.9939.

*2.8 [{Co(NCS)$_2$(**6**)$_2$}·4CHCl$_3$]$_n$*

$C_{52}H_{42}Cl_{12}CoN_8O_2S_2$, M = 1359.46, pink block, monoclinic, space group $P2_1/n$, a = 11.3206(10), b = 15.9765(14), c = 16.5480(14) Å, β = 91.496(4)°, U = 2991.9(3) Å^3, Z = 2, D_c = 1.509 Mg m^{-3}, μ(Cu-Kα) = 8.216 mm^{-1}, T = 123 K. Total 18554 reflections, 5365 unique, R_{int} = 0.139. Refinement of 5024 reflections (385 parameters) with I >2σ (I) converged at final R1 = 0.1118 (R1 all data = 0.1134), wR2 = 0.2308 (wR2 all data = 0.2310), gof = 1.0458.

*2.9 [{Co(NCS)$_2$(**7**)$_2$}·4CHCl$_3$]$_n$*

$C_{54}H_{46}Cl_{12}CoN_8O_2S_2$, M = 1387.47, pink block, monoclinic, space group $P2_1/n$, a = 11.7747(11), b = 15.5746(15), c = 16.6739(15) Å, β = 93.870(7)°, U = 3050.8(3) Å^3, Z = 2, D_c = 1.51 Mg m^{-3}, μ(Cu-Kα) = 8.070 mm^{-1}, T = 123 K. Total 5909 reflections, 5248 unique, R_{int} = 0.053. Refinement of 4479 reflections (331 parameters) with I >2σ (I) converged at final R1 = 0.1112 (R1 all data = 0.1236), wR2 = 0.2753 (wR2 all data = 0.2832), gof = 0.9761.

*2.10 [{Co(NCS)$_2$(**1**)$_2$}·0.5H$_2$O]$_n$*

$C_{40}H_{39}CoN_8O_{0.50}S_2$, M = 762.87, pink block, monoclinic, space group $C2/c$, a = 37.272(4), b = 11.9575(12), c = 23.770(3) Å, β = 125.290(6)°, U = 8647.3(17) Å^3, Z = 8, D_c = 1.172 Mg m^{-3}, μ(Cu-Kα) = 4.302 mm^{-1}, T = 123 K. Total 33334 reflections,

7564 unique, R_{int} = 0.117. Refinement of 2975 reflections (469 parameters) with $I > 2\sigma(I)$ converged at final $R1$ = 0.1514 ($R1$ all data = 0.2634), $wR2$ = 0.3615 ($wR2$ all data = 0.4950), gof = 1.0612.

3. Results and discussion

3.1 (4,4)-Nets in $[\{Co_2(NCS)_4(\mathbf{5})_4\}\cdot 2CHCl_3\cdot 1.5MeOH]_n$, $[\{Co(NCS)_2(\mathbf{6})_2\}\cdot 4CHCl_3]_n$ and $[\{Co(NCS)_2(\mathbf{7})_2\}\cdot 4CHCl_3]_n$

The assembly of crystalline coordination polymers with $Co(NCS)_2$ and ligands **5**, **6** and **7** was achieved by crystal growth by solution layering at room temperature. In each crystallization tube, pink crystals grew within 2 weeks. Ligands **5**, **6** or **7** (Scheme 3) differ only in the length of the peripheral alkoxy chain (methyl, ethyl, *n*-propyl). Each combination of **5**, **6** or **7** with $Co(NCS)_2$ leads to a (4,4) net. We first consider the details of the networks, and then evaluate the effects of increasing the length of the 4'-alkoxy tail on the interactions between the sheets in each lattice.

The complex $[\{Co_2(NCS)_4(\mathbf{5})_4\}\cdot 2CHCl_3\cdot 1.5MeOH]_n$ crystallizes in the triclinic space group *P*–1 with two independent cobalt atoms and four independent ligands in the asymmetric unit (Fig. 1). Each Co atom is octahedral, coordinated by *trans N*-thiocyanato ligands and by one outer pyridine donor of each of four separate **5** ligands. All Co–N bond lengths (caption to Fig. 1) and the angles within the metal coordination sphere are unexceptional. The sulfur atom in the $[NCS]^-$ ligand containing S118 (Fig. 1) is disordered and was modelled over two sites of fractional occupancies 0.60 and 0.40. The pyridine ring containing N67 is also disordered and was modelled over sites of 0.75 and 0.25 occupancies, with atoms N67 and C64 common to both positions. Each ligand **5** bridges two Co atoms (Fig. 1) and the structure consequently extends to the (4,4) net shown in Fig. 2. Bridged Co---Co distances lie in the range 12.613(2) to 13.193(2) Å,

and the internal angles of the two independent rhombuses in the net are 57.75(1) and 122.25(1)°, and 51.37(1) and 128.63(1)°.

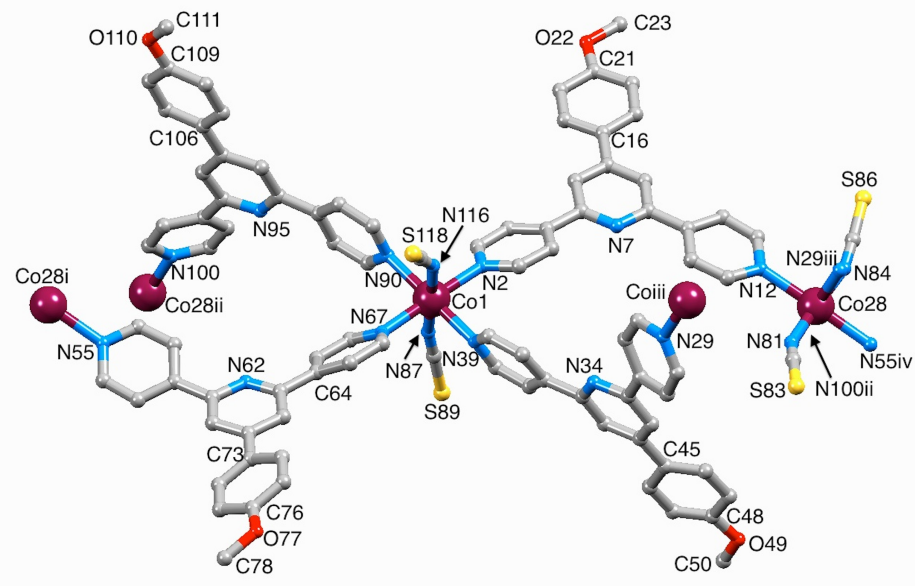

Fig. 1. The asymmetric unit of $[\{Co_2(NCS)_4(\mathbf{5})_4\}\cdot 2CHCl_3\cdot 1.5MeOH]_n$ with symmetry-generated atoms; H atoms and solvent molecules are omitted and only the major sites of the disordered sites (see text) are shown. Symmetry codes: i = 1+*x*, –1+*y*, *z*; ii = 1–*x*, –*y*, –*z*; iii = 1–*x*, 1–*y*, 1–*z*; iv = –1+*x*, 1+*y*, *z*. Atom $N100^{ii}$ is hidden under Co28. Selected bond distances: Co1–N2 = 2.208(4), Co1–N39 = 2.216(4), Co1–N87 = 2.069(5), Co1–N90 = 2.236(5), Co1–N116 = 2.087(5), Co1–N67 = 2.194(5), $Co28–N100^{ii}$ = 2.172(5), $Co28–N29^{iii}$ = 2.211(5), $Co28–N55^{iv}$ = 2.243(5), Co28–N81 = 2.077(5), Co28–N84 = 2.079(5) Å.

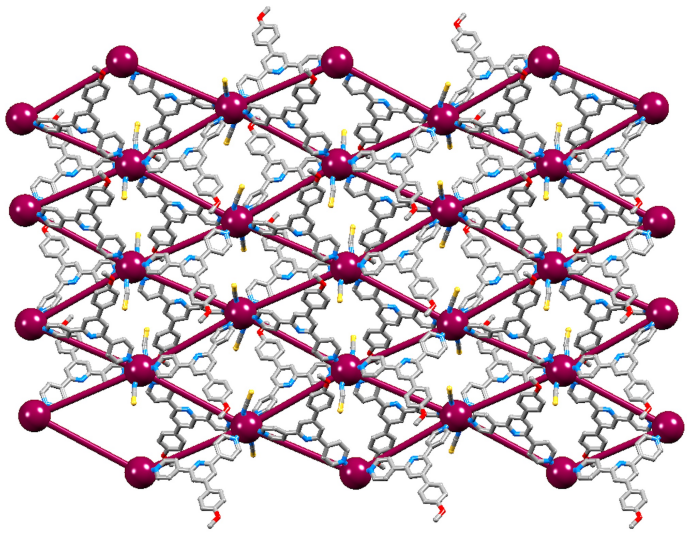

Fig. 2. Overlay of the structure and a TOPOS representation of part of the (4,4) net in $[\{Co_2(NCS)_4(\mathbf{5})_4\}\cdot 2CHCl_3\cdot 1.5MeOH]_n$; H atoms and solvent molecules are omitted.

Crystal growth by layering an MeOH solution of $Co(NCS)_2$ over a $CHCl_3$ solution of **6** or **7** resulted in the formation of $[\{Co(NCS)_2(\mathbf{L})_2\}\cdot 4CHCl_3]_n$ (**L** = **6** or **7**). Both coordination networks crystallize in the monoclinic space group $P2_1/n$ and possess very similar unit cell dimensions (see experimental section). The near-isostructural nature of $[\{Co(NCS)_2(\mathbf{6})_2\}\cdot 4CHCl_3]_n$ and $[\{Co(NCS)_2(\mathbf{7})_2\}\cdot 4CHCl_3]_n$ means that the structures are best considered together. Although the solvent region in $[\{Co(NCS)_2(\mathbf{7})_2\}\cdot 4CHCl_3]_n$ was partially treated using SQUEEZE [42], the consistency between the final solvent content of $[\{Co(NCS)_2(\mathbf{6})_2\}\cdot 4CHCl_3]_n$ and $[\{Co(NCS)_2(\mathbf{7})_2\}\cdot 4CHCl_3]_n$ supports the fitting of the electron density removed from the structure of $[\{Co(NCS)_2(\mathbf{7})_2\}\cdot 4CHCl_3]_n$ to two $CHCl_3$ molecules per Co atom. In each complex, atom Co1 is on an inversion centre; the structure of the repeat unit in $[\{Co(NCS)_2(\mathbf{6})_2\}\cdot 4CHCl_3]_n$ is shown in Fig. 3. The Co–N bond distances (Fig. 3, caption) are similar to analogous bond lengths in $[\{Co(NCS)_2(\mathbf{7})_2\}\cdot 4CHCl_3]_n$ (Co1–N_{tpy} = 2.217(4) and 2.165(4) Å, and Co1–N_{NCS} = 2.084(4) Å). In each structure, the sulfur atom of the $[NCS]^-$ ligand is disordered, and has been modelled over two sites (0.75/0.25 in $[\{Co(NCS)_2(\mathbf{6})_2\}\cdot 4CHCl_3]_n$, and 0.50/0.50 in $[\{Co(NCS)_2(\mathbf{7})_2\}\cdot 4CHCl_3]_n$). The Co---Co separations of 12.913(1) Å in $[\{Co(NCS)_2(\mathbf{6})_2\}\cdot 4CHCl_3]_n$ and 13.093(1) Å in $[\{Co(NCS)_2(\mathbf{7})_2\}\cdot 4CHCl_3]_n$ reflect the comparable spans of the 4,2':6',4''-tpy units in **6** and **7**, and lie within the range of bridged Co---Co separations (12.613(2) to 13.193(2) Å) in $[\{Co_2(NCS)_4(\mathbf{5})_4\}\cdot 2CHCl_3\cdot 1.5MeOH]_n$. The internal angles of the rhombus in the net in $[\{Co(NCS)_2(\mathbf{6})_2\}\cdot 4CHCl_3]_n$ are 103.57(1) and 76.43(1)°, and in $[\{Co(NCS)_2(\mathbf{7})_2\}\cdot 4CHCl_3]_n$ are 107.01(1) and 72.99(1)°, notably different from those in $[\{Co_2(NCS)_4(\mathbf{5})_4\}\cdot 2CHCl_3\cdot 1.5MeOH]_n$ (see above).

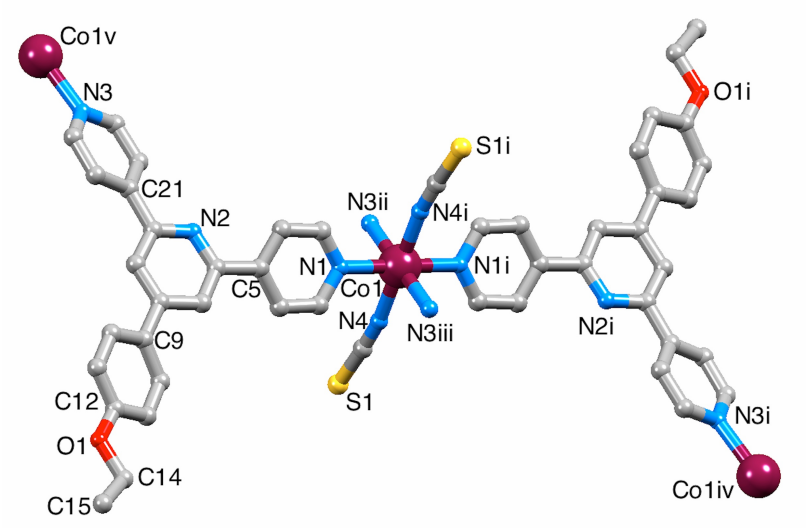

Fig. 3. The repeat unit in $[\{Co(NCS)_2(\mathbf{6})_2\}\cdot 4CHCl_3]_n$ including symmetry-generated atoms; H atoms and solvent molecules are omitted and only the major site of disordered atom S1 is shown. Symmetry codes: i = $-x$, $1-y$, $1-z$; ii = $^1/_2-x$, $^1/_2+y$, $^1/_2-z$; iii = $-^1/_2+x$, $^1/_2-y$, $^1/_2+z$; iv = $-^1/_2-x$, $^1/_2+y$, $^3/_2-z$; v = $^1/_2-x$, $-^1/_2+y$, $^1/_2-z$. Selected bond distances: Co1–N1 = 2.172(4), Co1–N4 = 2.063(4), Co1–N3^{ii} = 2.200(4) Å.

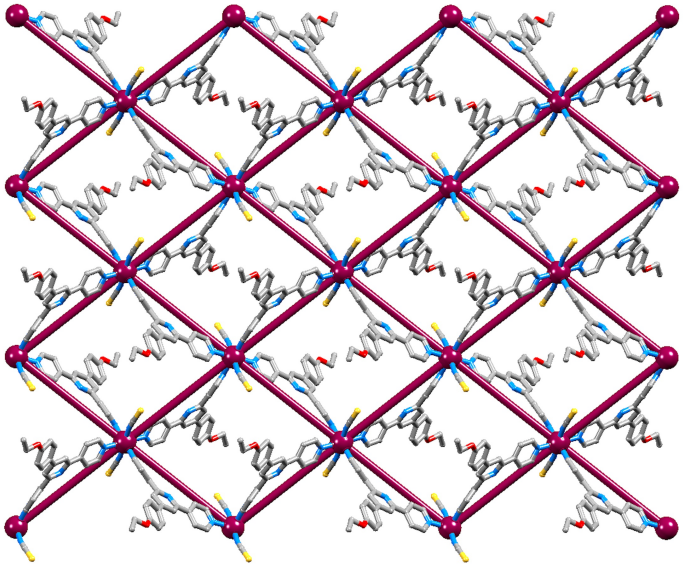

Fig. 4. Overlay of the structure and a TOPOS representation of part of the (4,4) net in $[\{Co(NCS)_2(\mathbf{6})_2\}\cdot 4CHCl_3]_n$; H atoms and solvent molecules are omitted.

In $[\{Co_2(NCS)_4(\mathbf{5})_4\}\cdot 2CHCl_3\cdot 1.5MeOH]_n$, $[\{Co(NCS)_2(\mathbf{6})_2\}\cdot 4CHCl_3]_n$ and $[\{Co(NCS)_2(\mathbf{7})_2\}\cdot 4CHCl_3]_n$, bridging ligands **5**, **6** or **7** are arranged in an up/up/down/down manner around each rhombus in the (4,4) net. In

$[\{Co_2(NCS)_4(\mathbf{5})_4\}\cdot 2CHCl_3\cdot 1.5MeOH]_n$, the ligands **5** are folded over the cavities in the net (Fig. 5a), while this is not the case in $[\{Co(NCS)_2(\mathbf{6})_2\}\cdot 4CHCl_3]_n$ (Fig. 5b) and $[\{Co(NCS)_2(\mathbf{7})_2\}\cdot 4CHCl_3]_n$. This is concomitant with a difference in packing of the (4,4) nets containing ligand **5** and those containing **6** or **7**. Sheets in $[\{Co_2(NCS)_4(\mathbf{5})_4\}\cdot 2CHCl_3\cdot 1.5MeOH]_n$ are interlocked as shown in Fig. 6a, with head-to-tail pairs of 4'-(4-methoxyphenyl)pyridine units from adjacent sheets involved in face-to-face interactions. There are four independent 4'-(4-methoxyphenyl)pyridine units in the asymmetric unit; two form π-stacked interactions with units in the sheet above, and two with 4'-(4-methoxyphenyl)pyridine units in the sheet below. In each head-to-tail pair, the 4'-(4-methoxyphenyl)pyridine units are arranged essentially as shown in Fig. 7a. As Fig. 7a shows, the π-stacking is not optimal due to slippage of the rings, as seen by the $phenyl_{centroid}...pyridine_{centroid}$ distance of 4.2 Å. Nonetheless, these interactions are the primary packing contacts between (4,4) nets.

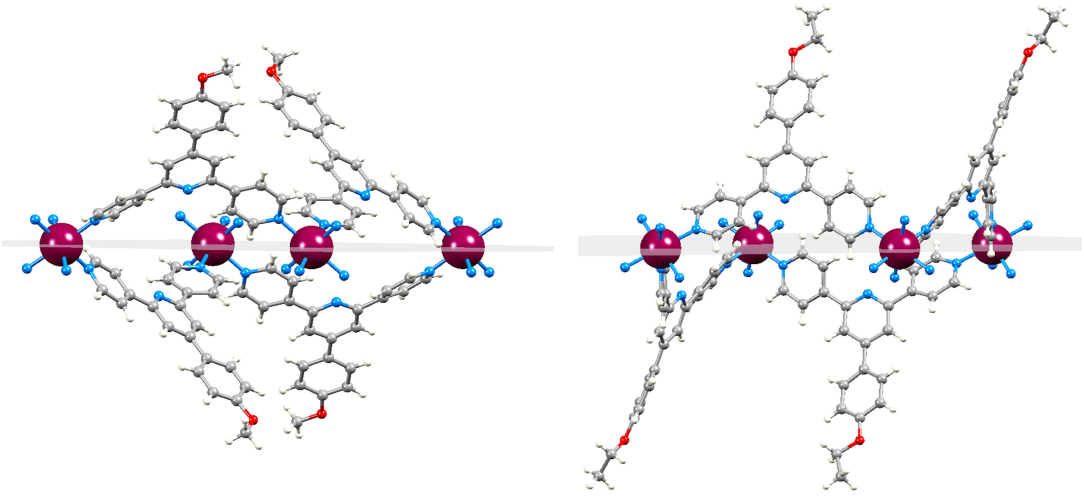

(a) (b)

Fig. 5. View through the plane of one metallomacrocycle in (a) $[\{Co_2(NCS)_4(\mathbf{5})_4\}\cdot 2CHCl_3\cdot 1.5MeOH]_n$ and (b) $[\{Co(NCS)_2(\mathbf{6})_2\}\cdot 4CHCl_3]_n$ showing the relative orientations of the bridging ligands with respect to the rhombus.

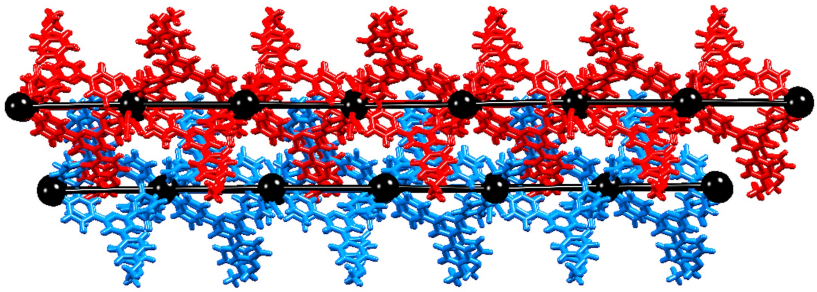

(a)

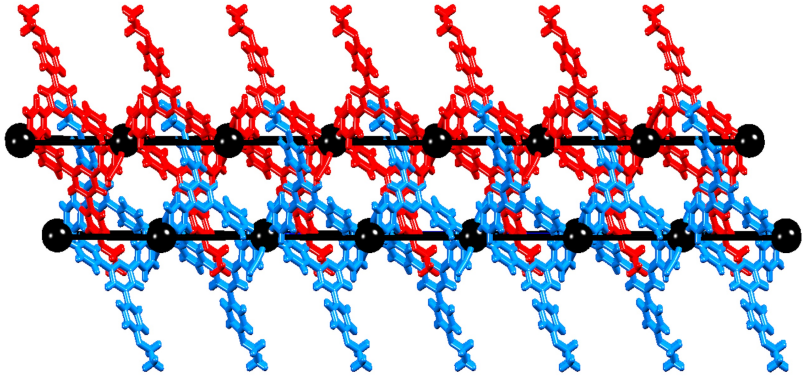

(b)

Fig. 6. Overlays of structures and TOPOS (in black) representations to show the packing of adjacent sheets (blue and red) in (a) $[\{Co_2(NCS)_4(\mathbf{5})_4\}\cdot 2CHCl_3\cdot 1.5MeOH]_n$ and (b) $[\{Co(NCS)_2(\mathbf{6})_2\}\cdot 4CHCl_3]_n$.

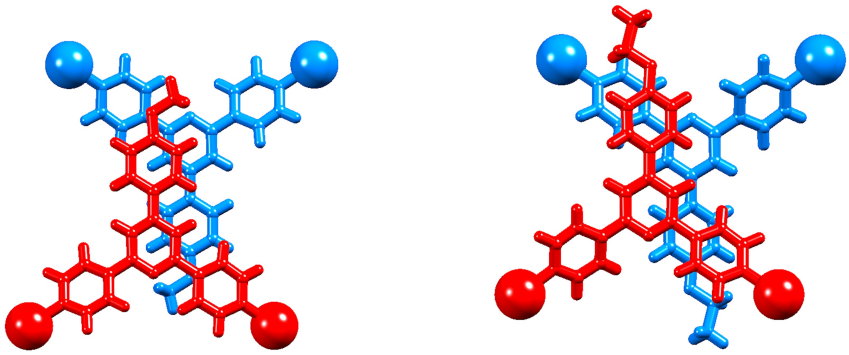

(a) (b)

Fig. 7. Face-to-face contacts between 4'-(4-alkoxyphenyl)pyridine units from adjacent sheets in (a) $[\{Co_2(NCS)_4(\mathbf{5})_4\}\cdot 2CHCl_3\cdot 1.5MeOH]_n$ (methoxy tails) and (b) $[\{Co(NCS)_2(\mathbf{6})_2\}\cdot 4CHCl_3]_n$ (ethoxy tails).

In $[\{Co(NCS)_2(\mathbf{6})_2\}\cdot 4CHCl_3]_n$ and $[\{Co(NCS)_2(\mathbf{7})_2\}\cdot 4CHCl_3]_n$, the 4-ethoxyphenyl (in **6**) or 4-*n*-propoxyphenyl (in **7**) units penetrate the adjacent sheet as shown in Fig. 6b. Head-to-tail π-stacking interactions between 4'-(4-alkoxyphenyl)pyridine units are the dominant packing forces between (4,4) nets in the complexes containing **6** and **7**, but differ from those involving **5** as can be seen by comparing Figs. 7a and 7b; for **5** the phenyl ring interacts with the middle pyridine ring of the 4,2':6',4''-tpy unit, but a slippage in the packing motif on going to the coordination polymers with **6** or **7** (Fig. 7) results in the phenyl ring lying over the outer pyridine ring of the 4,2':6',4''-tpy. As in $[\{Co_2(NCS)_4(\mathbf{5})_4\}\cdot 2CHCl_3\cdot 1.5MeOH]_n$, the orientations of the stacked arene rings are not ideal in $[\{Co(NCS)_2(\mathbf{6})_2\}\cdot 4CHCl_3]_n$, leading to ineffective π-contacts; the angle between the ring planes is 18.7° and the $phenyl_{centroid}...pyridine_{centroid}$ distance is 4.1 Å. These parameters are 25.2° and 4.2 Å in $[\{Co(NCS)_2(\mathbf{7})_2\}\cdot 4CHCl_3]_n$. The translational shift on going from one head-to-tail embrace to the other in Fig. 7 is reminiscent of the variation in π-stacking interactions between 4'-phenyl-2,2':6',2''-tpy domains in $[M(4'\text{-phenyl-2,2':6',2''-tpy})_2]^{2+}$ complexes discussed by McMurtrie and Dance [43].

In each of the (4,4) nets described above, the Co atoms are essentially coplanar. The differences in packing of adjacent sheets shown in Fig. 6 lead to only slightly larger inter-plane distances in $[\{Co(NCS)_2(\mathbf{6})_2\}\cdot 4CHCl_3]_n$ (9.228 Å) and $[\{Co(NCS)_2(\mathbf{7})_2\}\cdot 4CHCl_3]_n$ (9.305 Å) compared to $[\{Co_2(NCS)_4(\mathbf{5})_4\}\cdot 2CHCl_3\cdot 1.5MeOH]_n$ (8.936 Å). However, the penetration of the longer alkoxy chains through the holes in the adjacent sheets results in an offset ABAB.... arrangement of sheets in $[\{Co(NCS)_2(\mathbf{6})_2\}\cdot 4CHCl_3]_n$ and $[\{Co(NCS)_2(\mathbf{7})_2\}\cdot 4CHCl_3]_n$ with the closest Co...Co inter-net distances of 11.320(1) and 11.775(1) Å, respectively. In $[\{Co_2(NCS)_4(\mathbf{5})_4\}\cdot 2CHCl_3\cdot 1.5MeOH]_n$, the closest Co...Co inter-net distance is 9.414(1) Å.

After selection of an X-ray quality crystal, the remaining crystalline material for each of $[\{Co_2(NCS)_4(\mathbf{5})_4\}\cdot 2CHCl_3\cdot 1.5MeOH]_n$, $[\{Co(NCS)_2(\mathbf{6})_2\}\cdot 4CHCl_3]_n$ and $[\{Co(NCS)_2(\mathbf{7})_2\}\cdot 4CHCl_3]_n$ was subjected to powder diffraction for bulk sample analysis. However, after removal from the mother liquor, the pink crystals suffer solvent loss, becoming much paler. Figs. S1–S3 compare the powder diffraction patterns for the bulk samples with those predicted from the single crystal structures, and with powder patterns of $Co(NCS)_2$ and the respective free ligand **5**–**7**. For $[\{Co_2(NCS)_4(\mathbf{5})_4\}\cdot 2CHCl_3\cdot 1.5MeOH]_n$ and $[\{Co(NCS)_2(\mathbf{7})_2\}\cdot 4CHCl_3]_n$, characteristic peaks in the predicted patterns are present in the diffraction patterns of the bulk sample, in addition to other peaks. Free ligand is not present, confirming that the change in the crystalline sample occuring on exposure to air is due to simple solvent loss. For $[\{Co(NCS)_2(\mathbf{6})_2\}\cdot 4CHCl_3]_n$, the powder diffraction pattern for the bulk sample (Fig. S2) is ambiguous (taking into account shifts in peaks due to different data collection temperatures) and may contain free ligand **6**.

3.2 $[\{Co(NCS)_2(\mathbf{1})_2\}\cdot 0.5H_2O]_n$

X-ray quality crystals grown from the reaction between $Co(NCS)_2$ and **1** were extremely weakly diffracting. However, we have decided to give a brief description of the structure because of the interesting differences from that previously reported for the methanol solvate $[\{4Co(NCS)_2(\mathbf{1})_2\cdot MeOH\}\cdot H_2O]_n$ [17]. Layering of a MeOH solution of $Co(NCS)_2$ over a $CHCl_3$ solution of **1** led to pink crystals. An X-ray quality crystal was selected and structural determination confirmed the formation of $[\{Co(NCS)_2(\mathbf{1})_2\}\cdot 0.5H_2O]_n$. The X-ray diffraction powder pattern for the bulk sample is in good agreement with that predicted from the single crystal diffraction data (Fig. S4), confirming the homogeneity of the bulk material. The asymmetric unit contains two independent ligands **1** bound to atom Co1; this is octahedrally sited with *trans*-$[NCS]^-$ ligands (Fig. 8). Extension of the

structure generates a (4,4) net (Fig. 9a) in which each metallomacrocycle is characterized by bridged Co---Co separations of 13.414(4) and 13.198(4) Å and internal angles of 53.39(2) and 128.46(2)°. These angles are similar to those in $[\{Co_2(NCS)_4(\mathbf{5})_4\}\cdot 2CHCl_3\cdot 1.5MeOH]_n$ (see above).

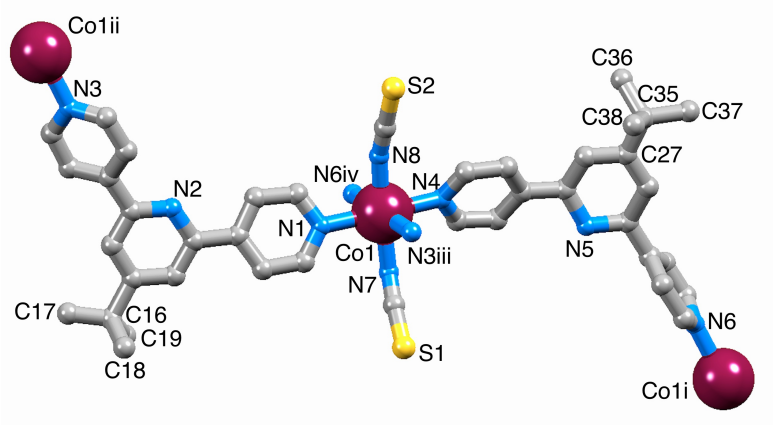

Fig. 8. The repeat unit in $[\{Co(NCS)_2(\mathbf{1})_2\}\cdot 0.5H_2O]_n$ including symmetry-generated atoms; H atoms and water molecules are omitted for clarity. Symmetry codes: i = *x*, 1–*y*, $^1/_2$–*z*; ii = *x*, –*y*, $-^1/_2$–*z*; iii = *x*, –*y*, $^1/_2$–*z*; iv = *x*, 1–*y*, $-^1/_2$–*z*. Selected bond lengths: Co1–N3^{iii} = 2.178(10), Co1–N6^{iv} = 2.165(10), Co1–N1 = 2.211(9), Co1–N4 = 2.181(9), Co1–N7 = 2.106(10), Co1–N8 = 2.078(10) Å.

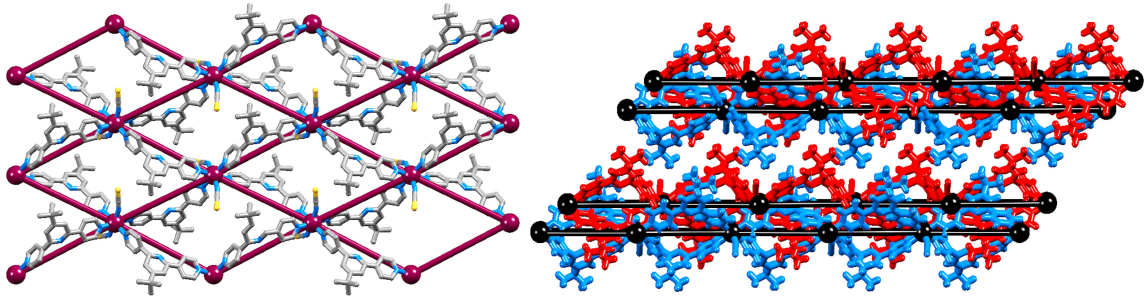

(a) (b)

Fig. 9 (a) Overlay of the structure and a TOPOS representation of part of the (4,4) net in $[\{Co(NCS)_2(\mathbf{1})_2\}\cdot 0.5H_2O]_n$; H atoms and solvent molecules are omitted. (b) View through four adjacent sheets (H atoms included) showing their short/long/short alternating separations; Co atoms and the (4,4) nets are shown in black. The (4,4) nets lie parallel to the *bc*-plane.

A comparison of the structures of $[\{Co(NCS)_2(\mathbf{1})_2\}\cdot 0.5H_2O]_n$ (this work) and $[\{4Co(NCS)_2(\mathbf{1})_2\cdot MeOH\}\cdot H_2O]_n$ [17] shows close similarities within a single (4,4) net, but significant differences in the packing of the nets. $[\{Co(NCS)_2(\mathbf{1})_2\}\cdot 0.5H_2O]_n$ and $[\{4Co(NCS)_2(\mathbf{1})_2\cdot MeOH\}\cdot H_2O]_n$ crystallize in the monoclinic space groups *C*2/*c* and *C*2, respectively. The angles in each rhombus in the net in $[\{Co(NCS)_2(\mathbf{1})_2\}\cdot 0.5H_2O]_n$ (53.39(2) and 128.46(2)^o) are close to those in $[\{4Co(NCS)_2(\mathbf{1})_2\cdot MeOH\}\cdot H_2O]_n$ (49.74(1) and 130.09(1)^o), and in both structures, the bridging ligands are organized in an up/up/down/down arrangement sequentially around a rhombus. In both structures, the Co atoms are coplanar, exactly so in $[\{Co(NCS)_2(\mathbf{1})_2\}\cdot 0.5H_2O]_n$ (a consequence of a translational symmetry operation) and within <0.3 Å in $[\{4Co(NCS)_2(\mathbf{1})_2\cdot MeOH\}\cdot H_2O]_n$. In the latter, the (4,4) nets lie directly over one another with closest Co---Co distances between sheets of 8.327(1) Å. In contrast, in $[\{Co(NCS)_2(\mathbf{1})_2\}\cdot 0.5H_2O]_n$, adjacent sheets are slipped, and have alternating wide and close spacings between adjacent nets as shown in Fig. 9b. For the short inter-net spacing, the Co---Co distances between adjacent nets are 7.715(1) and 9.214(1) Å, while for the longer inter-net spacing, the shortest Co---Co separations are 13.830(1) and 13.981(1) Å. We have previously described the inter-sheet interactions in $[\{4Co(NCS)_2(\mathbf{1})_2\cdot MeOH\}\cdot H_2O]_n$ as 'ball-and-socket packing' [17] with the *tert*-butyl groups accommodated in V-shaped cavities in the next sheet. In the newly reported structure of $[\{Co(NCS)_2(\mathbf{1})_2\}\cdot 0.5H_2O]_n$, the *tert*-butyl groups (shown in red in Fig. 10) face outwards from the pair of closely associated (4,4) nets, and result in hydrophobic layers filling the wider inter-sheet spacings.

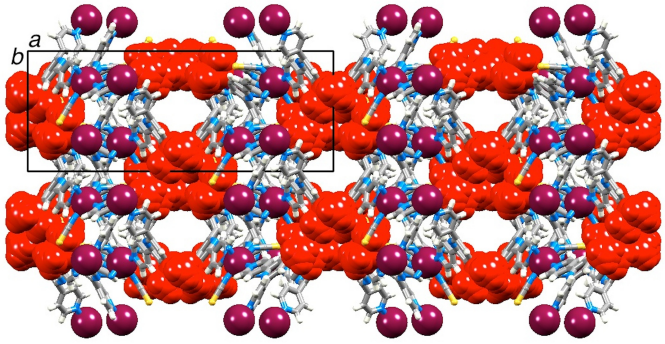

Fig. 10. Packing in $[\{Co(NCS)_2(\mathbf{1})_2\}\cdot 0.5H_2O]_n$ (viewed down the *c*-axis) with (4,4) nets parallel to the *bc*-plane; *tert*-butyl groups are shown in red space-filling representation.

4 Conclusions

We report four 2-dimensional (4,4) nets assembled through room termperature crystal growth experiments from reactions between $Co(NCS)_2$ and divergent 4,2':6',4''-terpyridine ligands **1**, **5**, **6** and **7**. The 2D-coordination networks in $[\{Co(NCS)_2(\mathbf{6})_2\}\cdot 4CHCl_3]_n$ and $[\{Co(NCS)_2(\mathbf{7})_2\}\cdot 4CHCl_3]_n$ are near isostructural and the internal angles in the rhombus in each net are 103.57(1) and 76.43(1)°, and 107.01(1) and 72.99(1)°, respectively. Although the (4,4) net in $[\{Co_2(NCS)_4(\mathbf{5})_4\}\cdot 2CHCl_3\cdot 1.5MeOH]_n$ is topologically the same as those containing **6** and **7**, the geometries of the rhombuses comprising the net are considerably different. Packing of sheets in all three coordination networks involves head-to-tail π-stacking of 4'-(4-alkoxyphenyl) units, but with variation in their relative orientations. In contrast, $[\{Co(NCS)_2(\mathbf{1})_2\}\cdot 0.5H_2O]_n$ consists of double layers of (4,4) nets with hydrophobic coatings of *tert*-butyl groups, leading to alternating wide and close spacings between adjacent nets. This contrasts with the previously reported structure of $[\{4Co(NCS)_2(\mathbf{1})_2\cdot MeOH\}\cdot H_2O]_n$ in which the (4,4) nets are equally spaced [17].

Appendix 1 Supplementary data

Crystallographic data for all the complexes have been deposited with the CCDC (Cambridge Crystallographic Data Centre, 12 Union Road, Cambridge CB2 1EZ, UK; fax +44 1223 336 033; e-mail: deposit@ccdc.cam.ac.uk or www: http://www.ccdc.cam.ac.uk) and may be obtained free of charge on quoting the deposition numbers CCDC 1407339–1407342.

Acknowledgements

We thank the Swiss National Science Foundation, the University of Basel, and the European Research Council (Advanced Grant 267816 LiLo) for financial support. The Swiss National Science Foundation through the NCCR Molecular Systems Engineering is acknowledged for partial funding of the powder diffractometer.

References

[1] M. Barquín, J. Cancela, M. J. González Garmendia, J. Quintanilla, U. Amador, Polyhedron 17 (1998) 2373.

[2] C. E. Housecroft, Dalton Trans. 43 (2014) 6594.

[3] F. Kröhnke, Synthesis (1976) 1.

[4] J. Wang, G. S. Hanan, Synlett (2005) 1251.

[5] Y.-Q. Chen, G.-R. Li, Z. Chang, Y.-K. Qu, Y.-H. Zhang, X.-H. Bu, Chem. Sci. 4 (2013) 3678 and references cited therein.

[6] C. Liu, Y.-B. Ding, X.-H. Shi, D. Zhang, M.-H. Hu, Y.-G. Yin, D. Li, Cryst.Growth Des. 9 (2009) 1275.

[7] P. Yang, M.-S. Wang, J.-J. Shen, M.-X. Li, Z.-X. Wang, M. Shao and X. He, Dalton Trans. 43 (2014) 1460 and references cited therein.

[8] F. Yuan, J. Xie, H.-M. Hu, C.-M. Yuan, B. Xu, M.-L. Yang, F.-X. Dong, G.-L. Xue, CrystEngComm 15 (2013) 1460 and references therein.

[9] Y. Li, Z. Ju, B. Wu, D. Yuan, Cryst. Growth Des. 13 (2013) 4125 and references therein.

[10] X. Tan, X. Chen, J. Zhang, C.-Y. Song, Dalton Trans. 41 (2012) 3616.

[11] Y. M. Klein, A. Prescimone, E. C. Constable, C. E. Housecroft, CrystEngComm (2015) doi: 10.1039/c5ce01115a.

[12] G. W. V. Cave, C. L. Raston, J. Chem. Soc., Perkin Trans. 1 (2001) 3258.

[13] J. Yoshida, S.-I. Nishikiori, H. Yuge, J. Coord. Chem. 66 (2013) 2191.

[14] S. A. S. Ghozlan, A. Z. A. Hassanien, Tetrahedron 58 (2002) 9423.

[15] E. C. Constable, C. E. Housecroft, S. Vujovic, J. A. Zampese, CrystEngComm 16 (2014) 3494.

[16] Y. M. Klein, E. C. Constable, C. E. Housecroft and A. Prescimone CrystEngComm 17 (2015) 2070

[17] E. C. Constable, C. E. Housecroft, P. Kopecky, M. Neuburger, J. A. Zampese, G. Zhang, CrystEngComm. 14 (2012) 446.

[18] E. C. Constable, C. E. Housecroft, M. Neuburger, S. Vujovic, J. A. Zampese, G. Zhang, CrystEngComm. 14 (2012) 3554.

[19] W. R. Knapp, D. P. Martin, R. L. LaDuca, Acta Crystallogr., E 63 (2007) m2745.

[20] D. M. Shin, I. S. Lee, D. Cho, Y. K. Chung, Inorg. Chem. 42 (2003) 7722.

[21] Z. Huang, H.-B. Song, M. Du, S.-T. Chen, X.-H. Bu, J. Ribas, Inorg. Chem. 43 (2004) 931.

[22] S. Wöhlert, I. Jess, C. Näther, Acta Crystallogr., Sect. E 69 (2013) m482.

[23] D. M. Shin, I. S. Lee, Y. K. Chung, M. S. Lah, Chem.Commun. (2003) 1036.

[24] H.-P. Wu, C. Janiak, L. Uehlin, P. Klüfers, P.Mayer, Chem. Commun. (1998) 2637.

[25] D. M. Shin, I. S. Lee, Y. K. Chung, Cryst. Growth Des. 6 (2006) 1059.

[26] M. Kondo, M. Shimamura, S. Noro, S. Minakoshi, A. Asami, K. Seki, S. Kitagawa, Chem.Mater. 12 (2000) 1288.

[27] L. M. Callejo, N. de la Pinta, G. Madariaga, L. Fidalgo, L. Lezama, R. Cortes, Cryst. Growth Des. 10 (2010) 4874.

[28] S. Wöhlert, J. Boeckmann, M. Wriedt, C. Näther, Angew. Chem. Int. Ed. 50 (2011) 6920.

[29] S. U. Son, B. Y. Kim, C. H. Choi, S. W. Lee, Y. S. Kim, Y. K. Chung, Chem. Commun. (2003) 2528.

[30] J. Lu, T. Paliwala, S. C. Lim, C. Yu, T. Niu, A. J. Jacobson, Inorg. Chem. 36 (1997) 923.

[31] L.-N. Zhu, Q.-L. Wang, W.-Z. Wang, D.-Z. Liao, Z.-H. Jiang, S.-P. Yan, J. Mol. Struct. 649 (2003) 111.

[32] B. Li, H. Liu, J. Chen, Z. Xu, Chem. Lett. (2001) 902.

[33] N. Masuhara, S. Hayami, N. Motokawa, A. Shuto, K. Inoue, Y. Maeda, Chem. Lett. 36 (2007) 90.

[34] S. M. Neville, G. J. Halder, K. S. Murray, B. Moubaraki, C. J. Kepert, Aust. J. Chem. 66 (2013) 452.

[35] Y. Inokuma, T. Arai, M. Fujita, Nature Chem. 2 (2010) 780.

[36] Y. M. Klein, E. C. Constable, C. E. Housecroft, J. A. Zampese, A. Crochet, CrystEngComm 16 (2014) 9915.

[37] Bruker Analytical X-ray Systems, Inc., 2006, APEX2, version 2 User Manual, M86-E01078, Madison, WI.

[38] P. W. Betteridge, J. R. Carruthers, R. I. Cooper, K. Prout, D. J. Watkin, J. Appl. Cryst. 36 (2003) 1487.

[39] I. J. Bruno, J. C. Cole, P. R. Edgington, M. K. Kessler, C. F. Macrae, P. McCabe, J. Pearson, R. Taylor, Acta Crystallogr., Sect. B 58 (2002) 389.

[40] C. F. Macrae, I. J. Bruno, J. A. Chisholm, P. R. Edgington, P. McCabe, E. Pidcock, L. Rodriguez-Monge, R. Taylor, J. van de Streek, P. A. Wood, J. Appl. Cryst. 41 (2008) 466.

[41] V. A. Blatov, A. P. Shevchenko, TOPOS Professional v. 4.0, Samara State University, Russia.

[42] A. L. Spek, Acta Crystallogr., Sect. D 65 (2009) 148.

[43] J. McMurtire, I. Dance, CrystEngComm 11 (2009) 1141.